Influence of Plastic Deformation on the Corrosion Behavior of Alloy 690TT in Crevice Condition of a Steam Generator

Ji-Young Han[a, b], Jin-Ho Park[a], Hee-Sang Shim[a], Sung-Woo Kim[a], Il Sohn[b], Soon-Hyeok Jeon[a*]
[a]*Materials Safety Technology Research Division, Korea Atomic Energy Research Institute, Daejeon, 34057, Korea*
[b]*Department of Materials Science and Engineering, Yonsei University, Seoul, 03722, Korea*
[*]*Corresponding author: junsoon@kaeri.re.kr*

Keywords : steam generator, Alloy 690, plastic deformation, corrosion behavior, crevice, impurity

1. Introduction

Alloy 690TT has a high corrosion resistance in the secondary water of pressurized water reactor (PWR). However, there still remains a potential problem that can damage the steam generator (SG) tubes. Notably, there are some dented tubes even in SGs with Alloy 690 thermally treated (TT) tubes [1,2]. Denting is another type of damage that affect the integrity of SG tubes, although it is not directly related to corrosion of the SG tube itself. The basic mechanism is that SG tubes are deformed from the outer to the inner surface by the volume expansion of the magnetite deposits caused by continuous corrosion of the tube support plate (TSP) or top of the tubesheet (TTS) in the crevices around the SG tubes [3]. Apart from the corrosion degradation of the SG tube itself, denting or tube deformation could lead to outer diameter stress corrosion cracking (ODSCC) in the tube. This degradation mechanism is affected by the concentration of impurities such as lead, chloride and sulfate ions, as well as oxidants in the crevices, leading to the corrosion acceleration of the tubesheet or TSP [1,2].

There are many investigations on ODSCC of SG tube materials in various crevice conditions. However, there have been few studies on the effects of plastic deformation on the general corrosion behavior and oxide formation of Alloy 690TT tubes in crevice condition of the SG.

In this study, the influence of plastic deformation on the general corrosion behavior of Alloy 690TT tubes was investigated in the high temperature crevice condition. To simulate the crevice condition of SGs, the various impurities such as Na, Cl, S, and, Pb were selected because these impurities was mainly observed in actual SG tube deposits. After corrosion tests, the corrosion rate of non-deformed and plastic deformed specimens were evaluated by weight change measurement. The microstructure of oxide particles was analyzed using a scanning electron microscope (SEM).

2. Methods

2.1 Specimens preparation

For the SG tube specimens for the corrosion tests, commercial Alloy 690TT tube was used. The chemical composition of Alloy 690TT tube used in this study is presented in Table I. Alloy 690TT specimens were machined in the form of a typical tensile test specimen.

To simulate the deformed SG tubes due to the volume expansion of the deposits, the specimens were elongated by about 15% and 30% by using tensile test.

After the tensile tests, the plastic deformed and non-deformed specimens were machined into two sizes: A size of 30 mm × 0.5 mm × 1.07 mm for weight change measurement and a size of 20 mm × 0.5 mm × 1 mm for microstructure analysis of oxide particles formed on Alloy 690TT after corrosion tests. The specimens were degreased in acetone and then in deionized water.

Table I: Chemical composition of Alloy 690TT tube (wt. %).

Cr	Fe	Si	Mn	Ti	Al	C	Ni
29.3	10.4	0.3	0.3	0.3	0.2	0.02	Bal.

2.2 Corrosion tests

Corrosion test was performed in the static Hastelloy C276 autoclave with a capacity of 1 gallon. In previous studies, the impurities such as Na, Cl, S, and Pb were observed on the crevice of SG deposits [2]. The type and concentration of impurities contained in the test solution was selected based on the EPRI report [4]. In order to accelerate the general corrosion test, the test solution is the mixed solution with 3 M NaCl, 0.35 M Na_2SO_4, 0.001 M NaOH, and 500 ppm PbO. The pH of test solution is 8.0 at 310 °C. The test solution was deaerated by purging of a mixed gas (10% hydrogen gas + 90% argon gas) and controlled at a hydrogen concentration of 6 ppm by injecting a mixed gas (5% hydrogen gas + 95% argon gas). The DO level was maintained below 5 ppb, a typical secondary waterchemistry guideline value [5]. After the temperature of solution was reached at 310 °C, the corrosion tests were conducted for three time intervals (250, 500, and 1000 h).

The gravimetric method was used to obtain corrosion rate from the corroded specimens. To evaluate the corrosion rate, the weight of the specimens before and after corrosion test was measured using microbalance with a resolution of 10^{-5} g. Before and after the

corrosion tests, each sample was measured three times and then averaged. The corrosion rates of the samples were calculated using the following relation:

$$\text{Corrosion rate (mg/cm}^2\text{·h)} = (W_b - W_a)/(A \times t)$$

where, A is the surface area of the specimen (cm^2), t is the test time (h), W_a is the weight of the sample before the test (mg). W_b is the weight of the sample after the test (mg).

2.3 Microstructure analysis

The specimens were grounded by SiC paper and electro-polished in the solution (90 vol.% methanol and 10 vol.% perchloric acid) at 30 V for 10 s. After that, the Kerneal Average Misorientation (KAM) and preferred orientation of specimens were analyzed by the SEM combined with electron back-scatter diffraction (EBSD) analyzer. Before and after the corrosion tests, the oxide particles formed on the three specimens (0, 15, and 30 % plastic deformed specimens) were observed using SEM.

3. Results

3.1 EBSD analysis of Alloy 690TT specimens

Fig. 1 shows the EBSD analysis results (001 IPF map and KAM map) of non-deformed and plastic deformed Alloy 690TT specimens. In the 001 IPF orientation map, a random orientation was observed (predominant orientation color did not appear). KAM map indicates that the crystal orientation deviation between a kernel center point and the neighboring points. As shown in Fig. 1, the misorientations of Alloy 690TT specimens do not exceed 5 °. KAM map of non-deformed specimen is blue color. However, KAM map of 15% and 30% plastic deformed specimens is mixed color with blue, green, and yellow. Average KAM results of three specimens (0%, 15%, and 30% plastic deformed specimens) were 0.11, 1.73, and 2.39 °, respectively. As the plastic deformation increased, the average KAM also increased because the plastic deformation increases the average direction deviation angle by inducing slip within the microstructure [6].

3.2 SEM analysis of Alloy 690TT specimens

Fig. 2 shows the SEM micrographs of non-deformed and plastic deformed Alloy 690TT specimens before the corrosion test. The non-deformed specimen was generally flat and smooth. No damage or cracks were observed on the surface of non-deformed specimen. However, the some damage or micro-cracks were observed on plastic deformed specimens. As the degree of deformation of specimen increased, the number of damage and cracks increased. During the plastic deformation process, the surface of Alloy 690TT specimen could be damaged such as strain concentration, void formation, and carbide fracture at grain boundaries [7].

In addition, the specimen surface becomes unstable due to the dislocation and slip of material atoms. We think that the damage and cracks formed on specimen surface could be affected on the corrosion behavior.

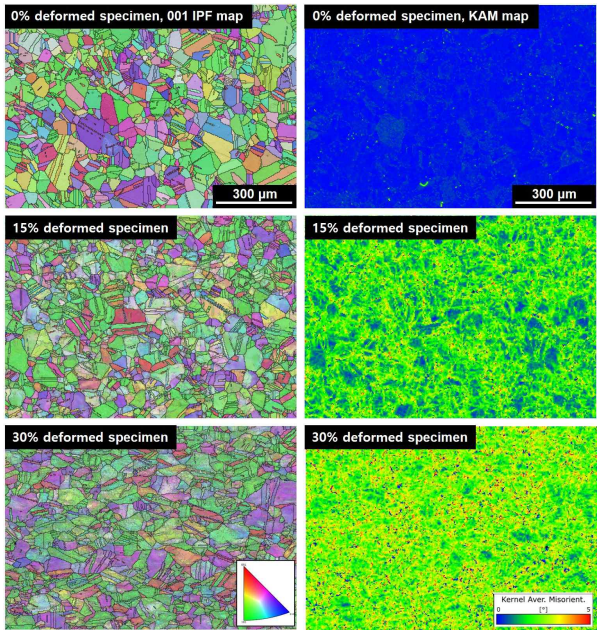

Fig. 1. EBSD analysis results of non-deformed and plastic deformed Alloy 690TT specimens.

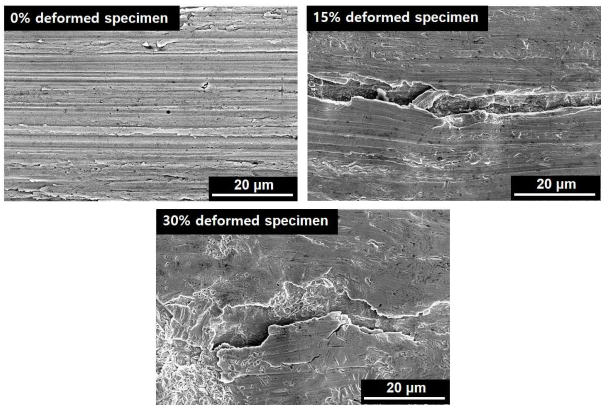

Fig. 2. SEM micrographs of surface of the specimens before the corrosion test.

Fig. 3 shows the SEM micrographs of non-deformed and plastic deformed Alloy 690TT specimens after the corrosion test for 1000 h. The planar-like oxides and polyhedral oxides were formed on all specimens. However, the oxide particles were more densely formed on the 30% plastic deformed specimen compared to the 0% plastic deformed specimen. In particular, the large polyhedral oxide particles with the size of about 5~6 μm were observed on 30% plastic deformed specimen.

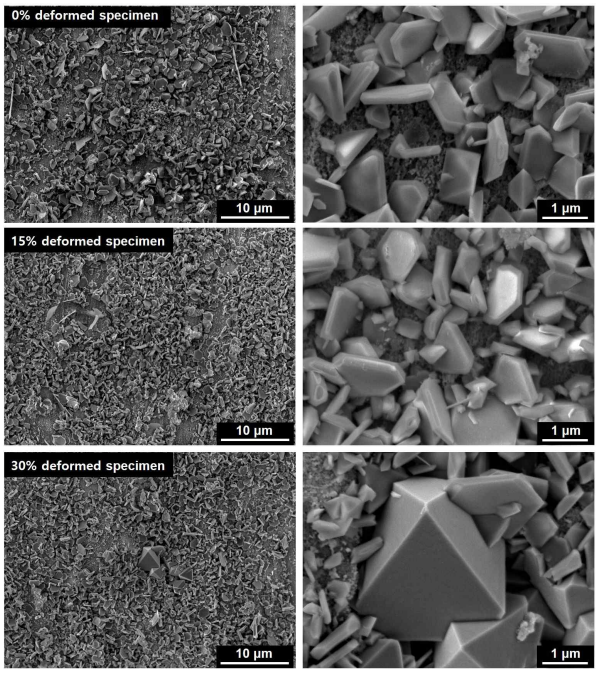

Fig. 3. SEM micrographs of surface of the specimens after the corrosion test for 1000 h.

These results indicate that the corrosion rate of Alloy 690TT specimen increased as the deformation degree of specimen increased.

Fig. 4 shows the corrosion rate of non-deformed and plastic deformed Alloy 690TT specimens in crevice condition. Under all specimens, the corrosion rate decreased with the increasing time. In the case of 500 h, compared to non-deformed specimen, the corrosion rate of 15% and 30% plastic deformed specimens increased by about 16% and 33%, respectively. Based on the results, the plastic deformation of Alloy 690TT specimen can affect the corrosion rate.

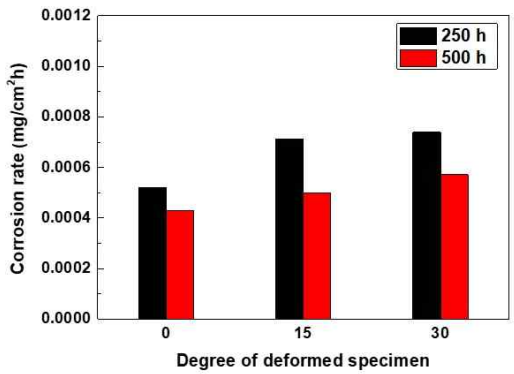

Fig. 4. Corrosion rate of non-deformed and plastic deformed Alloy 690TT specimens in crevice condition.

In the future, the chemical composition and chemical species of oxide layers formed on Alloy 690 specimens will be analyzed using focus ion beam (FIB)-SEM, X-ray diffraction, and X-ray photoelectron spectroscopy. The detailed results of oxide layer will be discussed at the oral presentation.

3. Conclusions

(1) Plastic deformation of Alloy 690TT greatly affects the change of microstructure. As the plastic deformation of specimen increased, the average KAM increased. Average KAM results of three specimens (0%, 15%, and 30% plastic deformed specimens) were 0.11, 1.73, and 2.39 °, respectively.
(2) The corrosion rate of Alloy 690TT tube increased with increasing the degree of plastic deformation due to the formation of surface damage and cracks.
(3) In the future, we will perform the electrochemical corrosion tests to evaluate the stability of passive film formed on non-deformed and plastic deformed specimens.

REFERENCES

[1] I. De Curieres, Environmental degradations in PWR steam generators. In Steam Generators for Nuclear Power Plants; Woodhead Publishing: Cambridge, UK, 2017.
[2] S. Choi, PWR steam generator tube denting at top of tubesheet, Paper 10137, In Proceedings of the International Conference on Nuclear Power Chemistry, Sapporo, Japan, p. 26–31 October. 2014.
[3] R.W. Staehle, J.A. Gorman, Quantitative assessment of submodes of stress corrosion cracking on the secondary side of steam generator tubing in pressurized water reactors: Part1. Corrosion, Vol.59, p. 931–944, 2003.
[4] B. Capell, Steam Generator Management Program: Assessment of Lead Induced Stress Corrosion Cracking Inhibitor Effectiveness, EPRI report 3002007860, Palo Alto, CA, USA, , 2016.
[5] K. Fruzzetti, Pressurized Water Reactor Secondary Water Chemistry Guidelines-Revision 8, EPRI report 3002010645, Palo Alto, CA, USA, , 2017.
[6] M. Kamaya, A.J. Wilkinson, J.M. Titchmarsh, Quantification of plastic strain of stainless steel and nickel alloy by electron backscatter diffraction, Acta Materiallia, Vol.54, p. 539–548, 2006.
[7] Q.J. Peng, J. Hou, T. Yonezawa, T. Shoji, Z.M. Zhang, F. Huang, E.-H. Han, W. Ke, Environmentally assisted crack growth in one-dimensionally cold worked Alloy 690TT in primary water, Corrosion Science, Vol.57, p. 81–88, 2012.